ELSEVIER

Cryogenics 40 (2000) 593–604

Cryogenics

www.elsevier.com/locate/cryogenics

Thermal-hydraulic analysis of T_{cs} measurement in conductor 1A of the ITER Central Solenoid Model Coil using the M&M code

L. Savoldi [1], R. Zanino *

Dipartimento di Energetica, Politecnico di Torino, 24, C.so Duca degli Abruzzi, 10129 Torino, Italy

Received 1 September 2000; accepted 10 January 2001

Abstract

We present a first study of current sharing temperature (T_{cs}) tests performed over the last few months in the Central Solenoid Model Coil (CSMC) experiment at JAERI, Naka, Japan. The CSMC is a superconducting magnet, layer-wound two-in-hand using 18 layers of Nb_3Sn two-channel cable-in-conduit conductors, which very recently reached a record 13 T at 46 kA DC operation. Here we apply the multi-conductor Mithrandir (M&M) code to a selected set of shots with different transport currents (30, 40, and 46 kA) and we concentrate on conductor 1A on the innermost (i.e., with highest magnetic field) layer. In the test, resistive heaters located upstream of layers 1 and 2 are used to progressively and quasi-steadily increase the supercritical helium inlet temperature in the coil. The T_{cs} is reached when a threshold of 0.5 mV resistive voltage is measured across the coil, after which the heaters are turned off and the coil current is dumped. Computed results are compared with experimental data, showing good agreement in the inlet and outlet temperatures of all four heated conductors, both as T_{cs} is reached (30, 40 kA) and during the whole hour-long transient from nominal conditions to T_{cs} reached (46 kA).

Keywords: Cable-in-conduit conductors; Superconducting cables; Fusion magnets

1. Introduction

The International Thermonuclear Experimental Reactor (ITER) model coils, i.e., central solenoid (CSMC) [1,2] and toroidal field (TFMC) [3,4], have been designed to test the conditions of operation of superconducting magnets which could be typical of a tokamak fusion reactor. In particular, the full testing campaign of the CSMC and of the CS insert has just been completed in August 2000 at the JAERI, Naka, facility in Japan, and the magnet has reached a number of operating records and provided a huge amount of data to analyze [5,6].

From the point of view of the modeling, the model coils constitute a formidable test-bed for thermal-hydraulic analysis. Based on previous experience, we can say that the requirements they impose on the computational tools are at least (more will become apparent during exercises like the present one...):

1. Availability of a suitable *2-fluid* description enabling the treatment of different thermodynamic state for the helium in the cable bundle region and the helium in the central channel (essential for the description of slow transients, e.g., heat slug injection [7,8], and also important for the accurate analysis of faster quench transients [9]);
2. Capability to account accurately enough for the *hydraulic/cryogenic circuit* external to the coil (essential for a self-consistent treatment of the problem, without any other inputs/drivers than those of the experiment itself) [10–12];
3. Capability to simultaneously describe *joint and conductor* (since thermal-hydraulic transients in the model coils are typically excited by resistive heaters located *outside* the coil) [13–15];
4. Capability to simultaneously describe *several conductors and their thermal coupling* (essential both in the joints, and for sufficiently slow/long transients also between turns and between layers) [16,17].

Here we present a study of current sharing temperature (T_{cs}) measurement in conductor 1A of the CSMC,

* Corresponding author. Tel.: +39-011-564-4490; fax: +39-011-564-4499.

E-mail addresses: savoldi@polito.it (L. Savoldi), zanino@polito.it (R. Zanino).

[1] Tel.: +39-011-564-4447.

0011-2275/01/$ - see front matter
PII: S0011-2275(01)00017-0

Nomenclature

(A)	set of critical parameters of the strands, as suggested in [18]
(B)	set of critical parameters of the strands, as suggested in [30]
B	magnetic field (T)
B_{c20m}	upper critical field at $T = 0$ (T)
C_0	normalization constant for the critical current density (A T/m^2)
CV	control valve in the cryogenic circuit
I	transport current (A)
M	generic manifold in the cryogenic circuit
n	value of the exponent in the power law model for the V–I characteristic of a strand
p	helium pressure (Pa)
t	time (s)
T	temperature (K)
T_B	bundle helium temperature (K)
T_{c0m}	critical temperature at $B = 0$ (K)
T_{cs}	current sharing temperature (K)
T_H	central channel helium temperature (K)
T_{in}	temperature at the inlet of conductor 1A (K)
T_{out}	temperature at the outlet of conductor 1A (K)
T_{st}	strand temperature (K)
V	voltage (V)
x	spatial coordinate along the conductor axis (m)

Greeks

ε	strand strain
ρ	helium density (kg/m^3)
τ_H	time constant for the thermal coupling between the inner module heaters and the helium (s)
ξ	head loss factor of the control valve

performed with the multi-conductor Mithrandir (M&M) code [17] – arguably the most complete validated tool available at present for this kind of analysis. This study follows a predictive steady-state analysis [16] of the same problem, performed with a simple semi-analytical model, where some account was given of the thermal coupling between different layers. The latter model was recently extended for interpretation of the data including some joint effects [18].

The paper is organized as follows. In the next section the experimental setup and testing procedure are briefly reviewed. We then discuss the model developed for this analysis, with particular reference to the cryogenic circuit of which the CSMC is the major component, and to the description of the thermal coupling inside the CSMC winding. A set of three experimental shots is then discussed, characterized by transport currents of 30 kA (shot # 051-002), 40 kA (shot # 048-002), and 46 kA (shot # 038-002), respectively, and the results of the computational analysis are compared with the test results. Based on this comparison, conclusions are drawn together with some comments on possible future work, which could be performed in perspective.

2. Brief overview of experimental setup and T_{cs} test procedure

We shall give here a short account of the experimental procedure, which will be presented elsewhere in full detail [19]. The CSMC is layer-wound two-in-hand using two-channel cable-in-conduit Nb_3Sn superconductors with thick, square Incoloy jacket. Layers are numbered from 1 to 18, starting from the innermost one. The first 10 layers constitute the so-called inner module, of US fabrication, while the eight remaining layers constitute the outer module, of Japanese fabrication. For each layer, the two conductors in hand are identified by A and B. The CS insert coil has been tested in the bore of the model coil and other inserts are planned to follow in the future.

Among the numerous tests which were performed on the CSMC over the last four months [20], we shall concentrate here on a subset of the T_{cs} tests performed on conductor 1A, where the highest magnetic field ($\sim$13 T at 46 kA) is located. (Only the test at 1 kA will not be considered here. In this case the normal zone is initiated at the inlet, with T_{cs} essentially equal to the measured inlet temperature, which makes it not very interesting for analysis).

Field maps [21] show that for the first layers the peak field is located near the midpoint of the conductor, while it tends to move towards the ends for increasing layer index, and is located there for all layers beyond 7. Considering that the only available sensors in the CSMC are located outside the coil [22], and in particular that the temperature sensors are located near the inlet and outlet of each conductor (see Fig. 1), the T_{cs} measurement is necessarily indirect for all layers where the peak field is not near its inlet/outlet, as in our case. A suitable analysis tool is therefore needed for a proper interpretation of the test results.

At any given current, the inlet temperature to conductor 1A was raised from its nominal value of 4.5 K, using two resistive heaters common to both layers 1 and 2 (see Fig. 1).

The tests were conducted in a quasi-steady fashion, increasing the heater power by successively smaller steps with long plateaus in between (see Fig. 2), allowing a new steady-state temperature profile along the conductors to be approximately reached for any power level after the first few steps. This strategy, considered safer

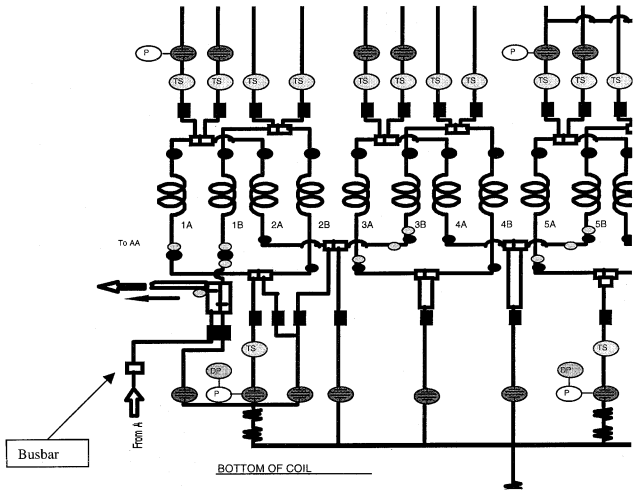

Fig. 1. Schematic of the CSMC hydraulic circuit (detail of innermost conductors in inner module). Helium flow is from bottom to top. Notice the heaters on the inlet plumbing common to conductor 1A, 1B, 2A, 2B, the joints (open rectangles), and the location of the temperature (TS), pressure (P) and flow sensors. Reproduced with permission from [18].

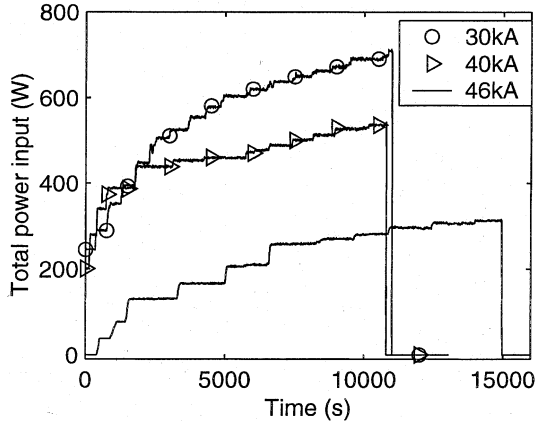

Fig. 2. Evolution of the input power from the resistive heaters at the common inlet of layers 1–2, for different transport currents $I = 30$ kA (○), 40 kA (▷), 46 kA (solid line). As the 0.5 mV threshold in resistive voltage (i.e., T_{cs}) is reached, the heaters are turned off.

than others intrinsically transient (e.g., heat slug injection) in reducing the uncertainty in the interpretation of the results, and possibly intrinsically more suited to the CSMC case where the peak field region is tens of meters beyond the joint, worked indeed very well, although leading to long tests requiring several hours each for completion. [2]

[2] At a mass flow rate ~4–5 g/s, with $p \sim 0.6$ MPa and $T \sim 5$–8 K, the helium density is ~100 kg/m^3, which combined with the flow area of ~$4–5 \times 10^{-4}$ m^2 [23], gives an average helium speed of 0.1 m/s and a helium residence time in the ~100 m long conductor of ~1000 s. This time is needed *after each power increase* to guarantee that a new steady state is reached.

Definition of the T_{cs} was based originally on the critical field criterion, 10 μV/m for 1 turn (~5 m long) = 0.05 mV resistive voltage. Eventually it was realized that the noise in the voltage signals was larger than expected and the threshold was increased by one order of magnitude to 0.5 mV. When this threshold was reached the heaters were switched off and the dump of the coil current was initiated. On two occasions, at 30 and 40 kA, an unexpected quench of the coil resulted, notwithstanding all precautions. An analysis of the quenches that occurred during the T_{cs} tests is beyond the scope of the present paper and will be presented elsewhere.

3. Description of the model

The model we apply to the analysis is based on the M&M code [17] for a detailed treatment of thermally coupled two-channel cable-in-conduit conductors, and on the Flower code [10,11] for the closure of the hydraulic/cryogenic circuit. Indeed, the CSMC experiment itself was one of the major motivations for the development of the M&M code once it was realized that existing tools with the capability of dealing only with a single conductor would not be suited to this case [23]. The major reason for this is that the time scale of interest of several experiments, including the T_{cs} test discussed here, is typically longer that the time scale needed for thermal coupling between turns and/or between layers to occur. In the following the main aspects of the circuit and of the coil model will be highlighted, and the simple model of resistive voltage and power generation will be reviewed.

3.1. Hydraulic/cryogenic circuit model

The cryogenic circuit, which feeds the CSMC, has been modeled as shown in Fig. 3(a). A volumetric pump provides a constant mass flow rate of supercritical helium at ~0.6 MPa and 4.5 K to the inlet manifold M1 (which includes cooling by the same amount as the work done by the pump). Helium then enters the CSMC winding (i.e., the parallel of all CSMC conductors, while insert coil and structure cooling circuit are neglected for the sake of simplicity) and flows out to manifold M2. From M2 the helium enters a heat exchanger, which brings it back to the nominal inlet conditions before entering the pump.

Concerning the CSMC winding, we have considered two options of different complexity for modeling different situations. The simpler model of Fig. 3(b) will be considered first and described below, while a discussion of the more complex model of Fig. 3(c) will be postponed until needed. Notice that both options, also in view of the different tools used in and the purpose of this

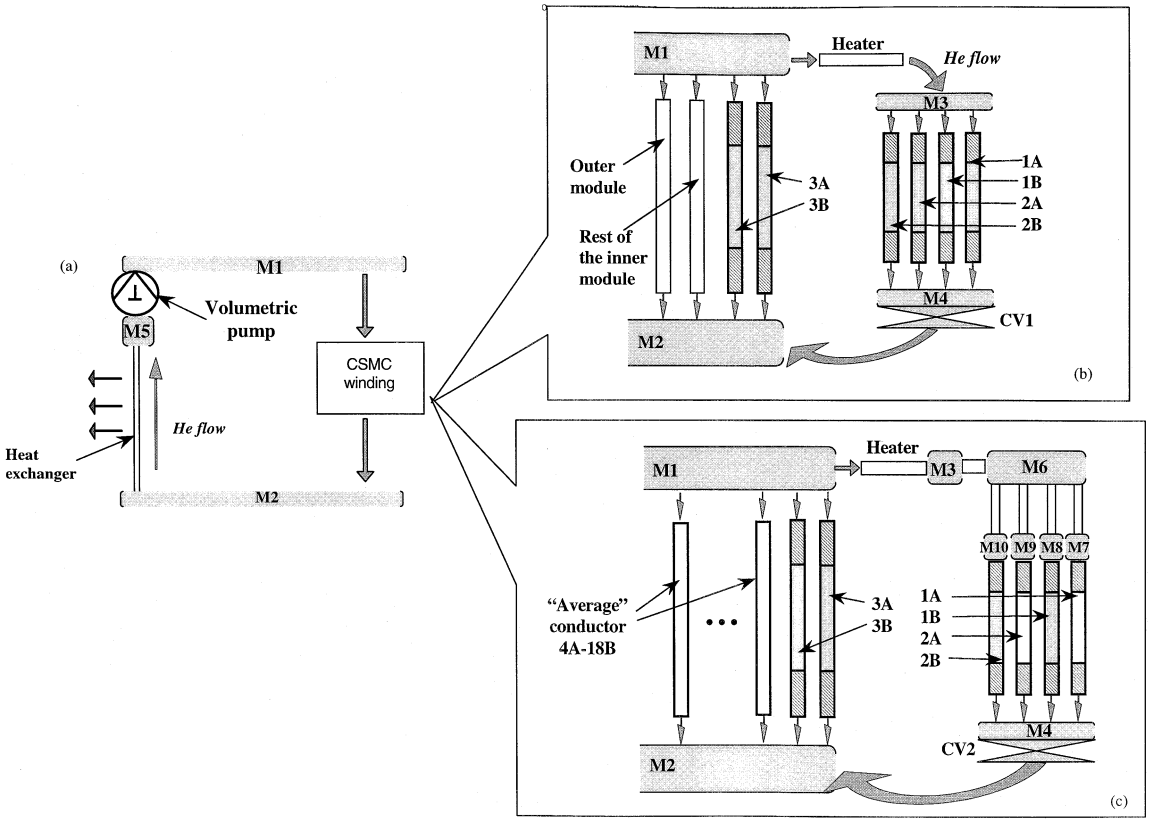

Fig. 3. Model of the cryogenic circuit used in the simulations. (a) Portion of the circuit feeding the CSMC winding, with the volumetric pump providing a constant mass flow rate to the winding. (b) Simple model of the CSMC winding. Conductors 1A–3B, and the busbar (not shown), are simulated with M&M, while the rest of the inner module and the whole outer module are simulated with Flower as incompressible pipes. The control valve CV1 has a constant head loss factor ξ. The heater is simulated with Flower as a compressible pipe. (c) More complex model of the CSMC winding. All conductors, and the busbar (not shown), are simulated with M&M.The ξ of control valve CV2 varies during the simulation following the experimental evolution. A more accurate description of the piping between the heater and the conductors of layers 1–2 is included.

study, significantly extend the circuit model previously presented in [24].

From the inlet manifold M1 a heated compressible pipe of Flower is used to simulate the two co-wound resistive heaters [22] located at the entrance of layers 1–2. [3] This feeds a manifold M3 from which the parallel of the four conductors 1A–B, 2A–B departs. The thermal coupling among these conductors and with the rest of the coil is most crucial to determine the temperature distribution during the tests. As can be seen from Fig. 1, conductor 1A is jointed with 2B, while 1B is jointed with the busbar, which is therefore modeled here also as a separate conductor. (The coupling 1B–busbar is indeed very important because the helium at the busbar inlet is always at nominal temperature and the temperature difference across that joint can therefore become relatively large [15], causing a significant reduction of the temperature in 1B between joint inlet and conductor inlet.) Conductor 2A is then jointed with 3B at the inlet. Notice that, since we need to use both inlet and outlet thermometer data, also the outlet joints need to be carefully modeled, i.e., we account here for the heat exchange in the joints between 1A–2A and 1B–2B. The heated helium is then collected in an outlet sub-manifold M4 and connected to the general outlet manifold M2 by a control valve CV1, which is used to regulate the mass flow rate in the heated layers 1–2. In the case of Fig. 3(b), CV1 is modeled with a *constant* head loss factor ξ [10,11], chosen ad-hoc such as to approximately reproduce the *initial* experimental mass flow rate in the heated layers 1–2 for a constant total mass flow rate forced by the volumetric pump.

Previous analysis with simplified models showed that inclusion of three [16] or four [18] thermally coupled layers should be enough to reproduce accurately the temperature distribution in layer 1, which is where the T_{cs} will appear first during these tests. Therefore in the case

[3] It is important to notice that, as opposed to the heaters used in the TFMC [25], a limited validation based on heat slug injection in conductor 1A (shot 032-002) showed that the inner module heaters are rather weakly coupled to the helium, with time constant ranging between 10 and 100 s. In the following simulations, therefore, the heater power deposited in the helium at each step increases exponentially to its plateau, with time constant $\tau_H = 72$ s.

of Fig. 3(b) we restrict the Mithrandir-like modeling to the first three layers + busbar (i.e., seven conductors in total) and model the rest of the inner module and the whole of the outer module with a single incompressible Flower pipe each.

Notice that, if needed, further subdivisions could be considered without principle difficulties, e.g., a separate pipe for layers 5–8 could be advised, with increased friction factor corresponding to the MIT spiral wire delimiting the central channel [26]. The latter indeed gives in the experiment much lower mass flow rates than in adjacent conductors of comparable length, but with the Showa flat spiral delimiting the central channel. However, the model of Fig. 3(b) will be used for the runs at 30 and 40 kA where, the initial power being different from zero (see Fig. 2), only the final phase of the transient will be followed in the simulations, i.e., when the voltage signal begins to leave the noise level, with the main target of reproducing the final spatial profiles in the different conductors. The evolution being limited, mass flow rate variations are also small, and even a relatively rough model of the circuit should be adequate.

3.2. Inter-turn and inter-layer coupling model

Concerning the first three layers we have attempted to take into account with the M&M code as much as possible of the complex topology of the CSMC [27]. We have modeled both inter-turn and inter-layer heat exchange, while no heat loss is accounted for in the buffer zone between the joints and the entrance of the coil.

The inter-turn coupling between conductors of the same layer is a *co-current* heat exchange along the upper and lower surfaces of the square jacket (see Fig. 4). Except for the first and last conductor turn, which are singular, each point on conductor A is coupled with the two points, respectively one turn ahead and one turn behind, on conductor B.

The topology of the inter-layer coupling is more complicated, as shown in Fig. 4, because two adjacent layers always have opposite pitch, in order to properly add their contribution to the magnetic field. This implies that: (i) each conductor "crosses" and therefore is coupled with both conductors of the adjacent layers, and (ii) the inter-layer heat exchange is *counter-current*.

For both inter-turn and inter-layer coupling, the heat transfer coefficient is computed as the series of the thermal resistances of the different insulation layers [17,22].

3.3. Simple model of resistive voltage and power generation

For the present analysis we have implemented in the M&M code the simple power-law model for the V–I characteristic of a strand, as given in [28], assuming the transport current to be uniformly distributed over the superconducting strands, and the field at the innermost line of each layer [21] to apply to the whole cross-section, for the sake of simplicity. From this, both the evolution of the resistive voltage and the Joule power generation in each unit length of conductor follow rather straightforwardly, once the parameter values B_{c20m}, T_{c0m}, C_0, and ε have been defined in the expression for the critical current [29], together with the value of the exponent n in the power law.

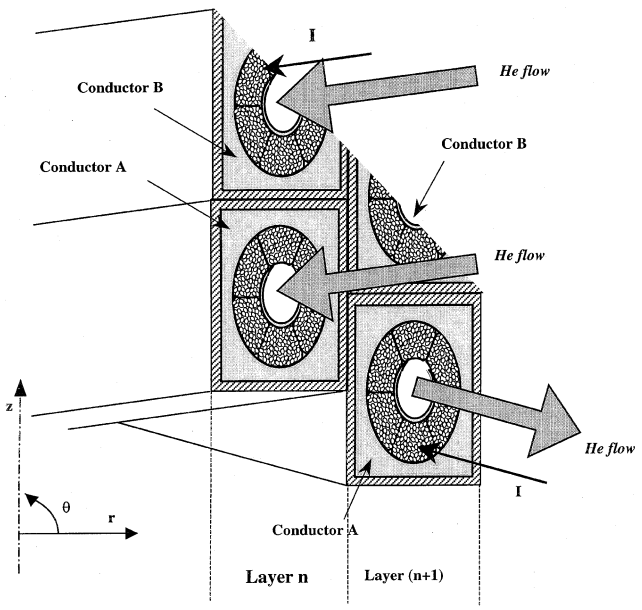

Fig. 4. Schematic view of the topology of the inter-turn and inter-layer heat exchange between adjacent conductors in the CSMC. A cross-section of two adjacent layers is shown on a vertical plane passing through the axis of the coil.

For the purpose of assessing the sensitivity of the model results, two different sets of parameters will be used in the following for B_{c20m}, T_{c0m}, C_0, and ε, both derived under somewhat different assumptions from CSMC T_{cs} data (the use of strand data only leads to inconsistencies with the CSMC data [30]), while $n = 20$ will be assumed based on strand data. The two sets are as follows:

(A)
$B_{c20m} = 28\ T$; $T_{c0m} = 18$ K; $C_0 = 0.94 \times 10^{10}$ AT/m^2 and $\varepsilon = -0.28\%$ [18];

(B)
$B_{c20m} = 27\ T$; $T_{c0m} = 18$ K; $C_0 = 0.75 \times 10^{10}$ AT/m^2 and $\varepsilon = -0.22\%$ [30].

Since the field distribution used in [30] is not available to us, we shall always use the field given in [21], which was also used to obtain set (A). No assessment of the relative merits of the two best-fits shall therefore be possible. Notice finally that, in principle, the very results for T_{cs} obtained in this paper could be used to iteratively find new best-fit values for the above-mentioned parameters, but this is beyond the scope of the paper.

4. Results and discussion

We shall now present the results of the simulation and compare them with the experimental data, separately for each transport current. In all cases with heated layers 1 and 2 experiment and simulations agree in having a normal zone initiation only in conductor 1A.

As said above we shall treat first the shots at 30 and 40 kA, using the circuit model of Fig. 3(b), and concentrating on the temperature profiles along different conductors as T_{cs} is reached, after an evolution over only the last few thousands of seconds of the actual transient (i.e., from $t = 8000$ s in Fig. 2). No attempt will be made for these shots to model the full thermal-hydraulic transients (i.e., from $t = 0$ s in Fig. 2) because their initial conditions are characterized by finite heater power and already result from hour-long regulation of heater power, pump rpm, and control valves.

In the third part of this section the shot at 46 kA will be analyzed. In view of the fact that it starts from zero heater power (see Fig. 2) we have attempted in this case to follow the full thermal-hydraulic transient from nominal initial conditions to T_{cs} reached. The fundamental role of hydraulic circuit modeling will be discussed by comparing the results obtained in this case with different circuits (see Figs. 3(b) and (c)). To the best of our knowledge this is the first example of a multiple-time-scale simulation for fusion magnets thermal-hydraulics, wherein one studies a very slow O(10^4 s) transient, followed by a relatively much faster O(10^2–10^3 s) evolution of the resistive voltage, leading to current sharing conditions.

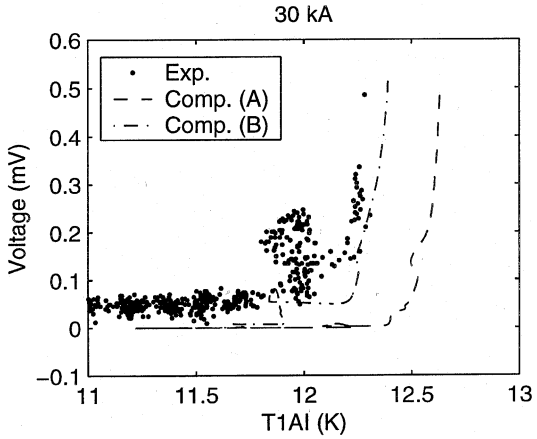

Fig. 5. T_{cs} measurement at $I = 30$ kA: computed voltage drop along conductor 1A, as a function of the temperature at conductor inlet, after the heaters. The results obtained using set (A) (dashed) and set (B) (dash-dotted) of critical current parameters (see text) are compared with experimental data obtained from voltage sensor MCI_VD_01A and temperature sensor MCI_TS_01AI (•).

4.1. Analysis of the 30 kA shot

The evolution of the voltage on conductor 1A is shown as a function of the inlet temperature in Fig. 5 for the two sets (A) and (B) of critical current parameters, and compared with the experimental data. The corresponding spatial profiles of the temperature along the conductor, when the computed voltage reaches 0.5 mV, are shown in Figs. 6 and 7 for the two sets (A) and (B), respectively, and compared with measured values at the inlet and outlet of conductors 1A, 1B, 2A, 2B. Of course, the agreement in voltage evolution can only be very qualitative in view of the rudimentary uniform current–uniform field assumptions in our model [28]. With respect to the results shown in [30] it has however to be observed that here also the inlet temperature is self-consistently computed, and not taken from the

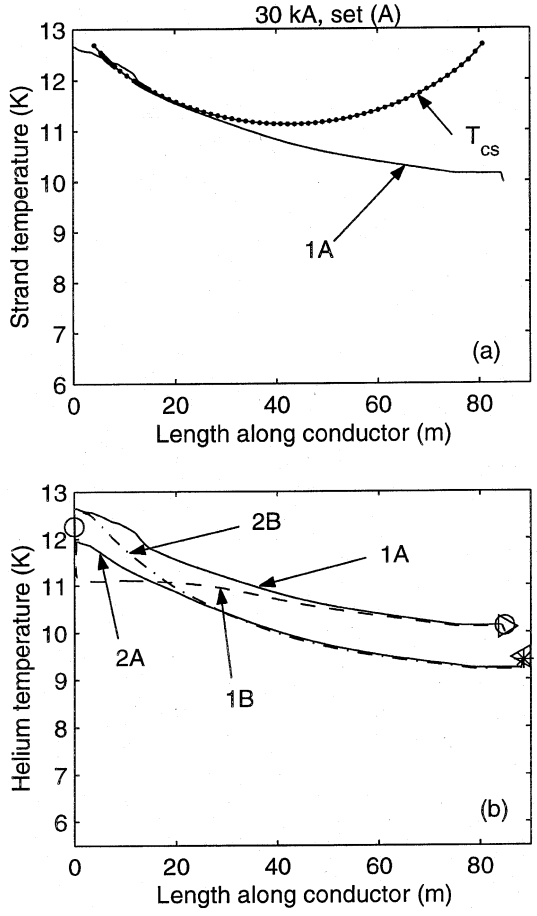

Fig. 6. T_{cs} measurement at $I = 30$ kA. Results computed using set (A). (a) Spatial profile of the strand temperature along conductor 1A (solid), at T_{cs} reached in the simulation. The profile of T_{cs} along the conductor is also reported (•). (b) Spatial profile of the average helium temperature along conductors 1A–2B at T_{cs} reached in the simulation, compared with temperatures measured at inlet, MCI_TS_01AI (○), and at outlet, MCI_TS_01AO (○), MCI_TS_01BO (▷), MCI_TS_02AO (∗) and MCI_TS_02BO (◁), in 1A, 1B, 2A, 2B, respectively, at T_{cs} reached in the experiment.

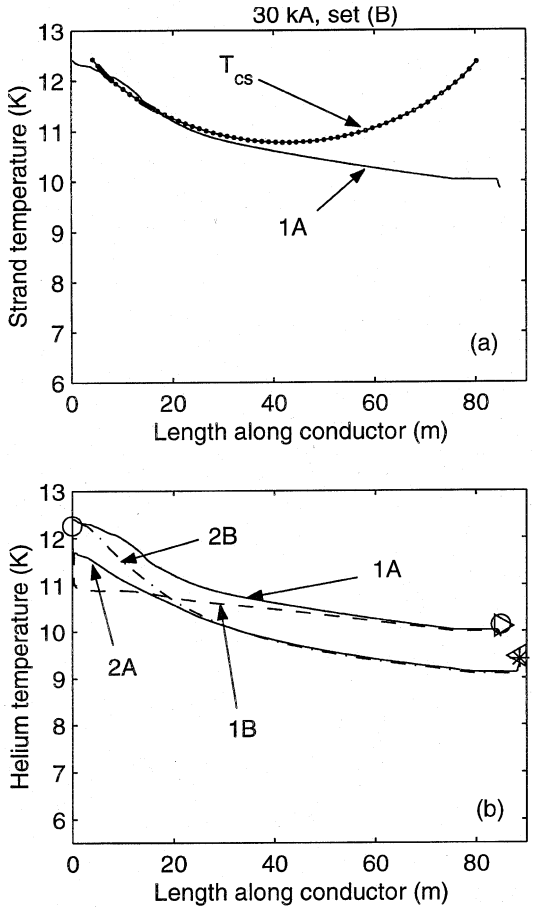

Fig. 7. T_{cs} measurement at $I = 30$ kA. Results computed using set (B). (a) Spatial profile of the strand temperature along conductor 1A (solid), at T_{cs} reached in the simulation. The profile of T_{cs} along the conductor is also reported (•). (b) Spatial profile of the average helium temperature along conductors 1A–2B at T_{cs} reached in the simulation, compared with temperatures measured at inlet, MCI_TS_01AI (○), and at outlet, MCI_TS_01AO (○), MCI_TS_01BO (▷), MCI_TS_02AO (∗) and MCI_TS_02BO (◁), in 1A, 1B, 2A, 2B, respectively, at T_{cs} reached in the experiment.

experiment as a boundary condition. From Figs. 6(a) and 7(a) it may be seen that, as expected from simple modeling [16], the normal zone is initiated relatively near the conductor inlet. As a measure of the accuracy of this prediction, and of the resulting T_{cs} of conductor 1A, one can see from Figs. 6(b) and 7(b) that inlet and outlet temperature values in different heated conductors are quantitatively well reproduced by the model. From Figs. 6(b) and 7(b) it can also be seen that a finite and relatively large gradient arises along the conductor because of heat exchange with adjacent layers. While inlet jumps are determined by the heat generation and exchange in the inlet joint (see below) strong inter-turn coupling leads to very similar outlet temperature in different conductors of the same layer, while the outlet temperature in layer 1 is higher than in layer 2 because of Joule heat generation in the normal zone. Notice finally that, as for the voltage evolution, a somewhat better agreement in inlet and outlet temperatures is obtained with set (B).

4.2. Analysis of the 40 kA shot

The evolution of the voltage between coil inlet and outlet in this case is shown as a function of the inlet temperature in Fig. 8, while in Fig. 9 we show the profiles obtained at the end of the simulation (coinciding with the time the input power is turned off in Fig. 2) with set (A). Notice from Fig. 8 that in this case the 0.5 mV threshold is not reached in the simulation while the heaters are still on. This is however borderline (see Fig. 9(a)) and the agreement between computed and experimental inlet and outlet temperatures appears to be good. Comparison of Fig. 9(a) with Fig. 7(a) shows also that the temperature gradient along the conductor is now significantly reduced, because the lower temperature gives lower *radial* temperature gradients in the coil, which implies lower radial heat losses. Concerning the behavior in the joints, zooms of the temperature profiles along the conductor are shown in Figs. 10(a), (b) (inlet) and (c) (outlet). At the inlet one notices an almost flat profile in 1A and 2B, since they are joined to each other and both heated (Fig. 1), with a slight temperature increase due to Joule heat generation there. In both 1B and 2A, on the other hand, one notices a strong drop of the strand temperature due to radial heat losses to busbar and 3B respectively (Fig. 1), followed by a significant recovery right after the joint. In order to understand the recovery one can further zoom along the first meter, including the joint (∼0.4 m long) and the very first portion of conductor, as shown in Fig. 10(b). It

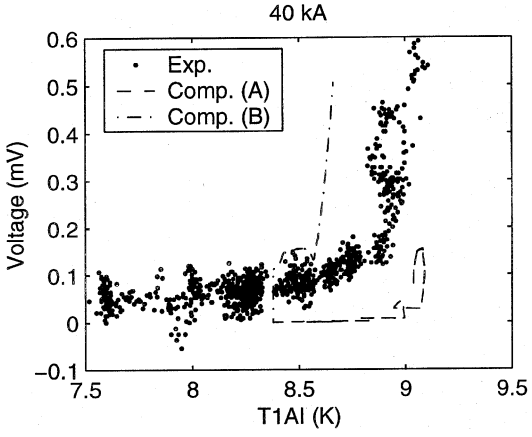

Fig. 8. T_{cs} measurement at $I = 40$ kA: computed voltage drop along conductor 1A, as a function of the temperature at conductor inlet, after the heaters. The results obtained using set (A) (dashed) and set (B) (dash-dotted) of critical current parameters (see text) are compared with experimental data obtained from voltage sensor MCI_VD_01A and temperature sensor MCI_TS_01AI (•). Notice that in the case of set (A) the 0.5 mV threshold is not reached in the simulation with the maximum experimental heating power, but this is rather borderline (see Fig. 9(a)).

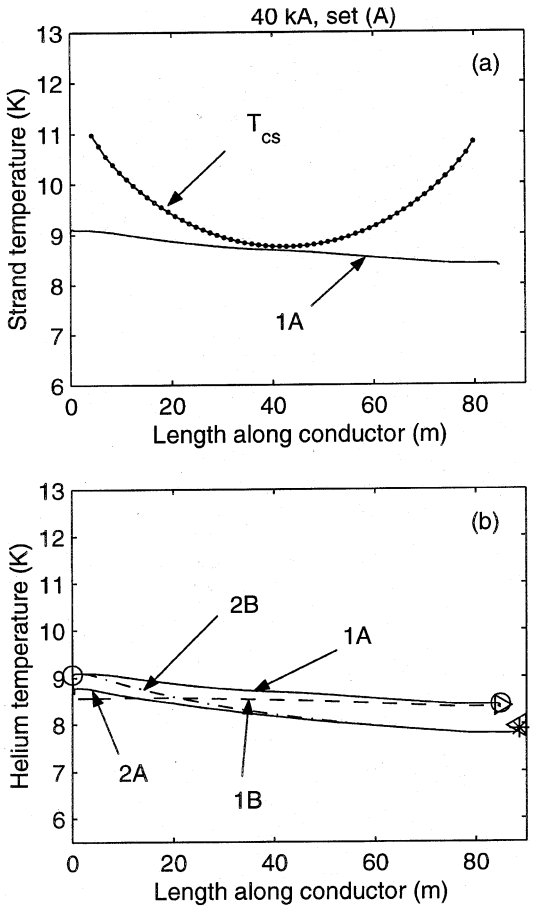

Fig. 9. T_{cs} measurement at $I = 40$ kA. Results computed using set (A). (a) Spatial profile of the strand temperature along conductor 1A (solid), at the end of the simulation. The profile of T_{cs} along the conductor is also reported (•). (b) Spatial profile of the average helium temperature along conductors 1A–2B at T_{cs} reached in the simulation, compared with temperatures measured at inlet, MCI_TS_01AI (○), and at outlet, MCI_TS_01AO (○), MCI_TS_01BO (▷), MCI_TS_02AO (∗) and MCI_TS_02BO (◁), in 1A, 1B, 2A, 2B, respectively, at T_{cs} reached in the experiment.

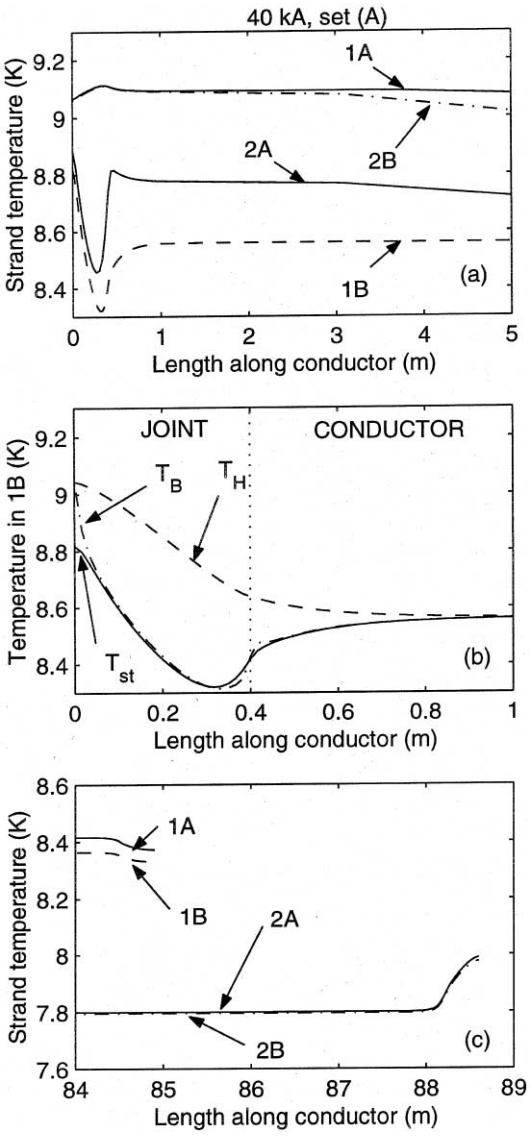

Fig. 10. T_{cs} measurement at $I = 40$ kA. Zooms near inlet and outlet of spatial profile of the solution obtained with set (A) at the end of the simulation. (a) Zoom of the spatial profile of strand temperature on the first 5 m at inlet of conductors 1A, 1B, 2A, 2B. (b) Zoom of the spatial profile of strand, bundle helium and hole helium temperature on the first meter at inlet of conductor 1B. (c) Zoom of the spatial profile of strand temperature on the last few meters at outlet of conductors 1A, 1B, 2A, 2B.

is seen that, according to the model, the drop of the bundle helium temperature T_B, due to the heat exchange through the jacket, pulls the strands, which are strongly coupled to it, while weaker coupling with the hole helium (H) gives a finite temperature gradient $T_H - T_B$. Once the joint, i.e., radial heat exchange, is over, the warmer helium in the hole heats the bundle helium and therefore the strands, which qualitatively explains the recovery. [4] At the outlet joint 1A is joined with 2A and 1B with 2B, so that both conductors in layer 1 cool down, heating their homologues in layer 2. The profiles are not anti-symmetric because of Joule heating in the outlet joint. Notice finally that the temperature reduction/increase in a joint is driven by the balance between heat generation, which dominates at high current, and heat exchange, which dominates at low current.

4.3. Analysis of the 46 kA shot

Since the history of the shot at 46 kA allows it (see Fig. 2) we attempted to simulate the full evolution of this

[4] Although this phenomenon was observed in tests of joint samples of the TFMC type [17], i.e., with thick tube delimiting the central channel in the joint, it was not possible yet to confirm it experimentally in tests of joint samples of the CSMC type [15], i.e., with the same spiral delimiting the central channel both in the joint and in the conductor, because of the lack of a temperature sensor right after the joint.

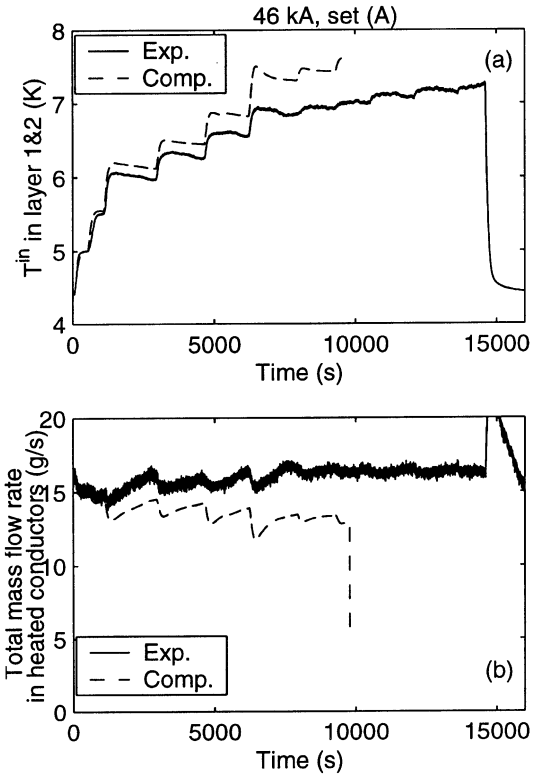

Fig. 11. T_{cs} measurement at $I=46$ kA. (a) Evolution of T_{in} (dashed), computed using the winding model in Fig. 3(b) and set (A), compared to the experimental signal from MCI_TS_01AI (solid). (b) Evolution of the total mass flow rate in heated conductors computed using the winding model in Fig. 3(b) and set (A) (dashed), compared to the total measured mass flow rate (sum of the signals from MCI_FCT_01AI, MCI_FCT_01BI, and MCI_FCT_02A02BI (solid)).

run with the winding model of Fig. 3(b). The result is compared with the experiment in terms of evolution of the inlet temperature (Fig. 11(a)) and of the total mass flow rate (Fig. 11(b)) to the heated conductors. We see that the simulation is inadequate to reproduce the experimental evolution, giving overestimated mass flow rate reduction and temperature increase at the heaters outlet.

In an attempt to improve this situation we modified the model of the CSMC winding as in Fig. 3(c). The major differences with respect to the circuit of Fig. 3(b) can be summarized as follows, in order of importance: (1) substitution of the control valve CV1, which had a constant ad-hoc head loss factor ξ (see above), with a control valve CV2 with experimentally calibrated characteristic; [5] (2) substitution of the two lumped incompressible pipes of Flower representing conductors 4A–10B and 11A–18B, respectively, with 30 "average" conductors; (3) inclusion of more accurate description of the piping between heater and inlet joints.

The result of the full evolution with the circuit of Fig. 3(c) is shown in Fig. 12 for the thermal-hydraulic variables and in Fig. 13 for the voltage, all subject to the simulated evolution of the power input into the helium as shown in Fig. 12(h). We notice that the accuracy of the evolution of the inlet temperature and mass flow rate to the heated layers (Figs. 12(a) and (e), respectively) is significantly improved, with respect to Figs. 11(a) and (b). Also the accuracy of the evolution of the outlet temperatures for layer 1 (Fig. 12(b)), layer 2 (Fig. 12(c)) and layer 3 (Fig. 12(d)) appears to be good. Some discrepancy is seen in the pressurization of the heated conductor (Fig. 12(f)). This can be a consequence of the rough estimation of the volume of the helium in the cryogenic circuit used to define M1 and M2. Again, the agreement in voltage evolution shown in Fig. 13 is only qualitative.

In Fig. 14 we show the temperature profiles along the heated conductors at the time when the computed voltage reaches 0.5 mV with parameter set (A). It is seen that the normal zone is initiated near the middle of the conductor length, and the profiles are even flatter than in the case of 40 kA (see above).

The results of the present analysis, summarized in terms of computed values of the T_{cs} corresponding to the 0.5 mV criterion, are shown in Table 1 for the two sets of critical current parameters (A) and (B). Notice that the simplistic estimate of T_{cs} based on the arithmetic average between experimental inlet and outlet temperatures (i.e., the only ones which have been measured) is within few tenths of a Kelvin from the computed results at high current, while this difference increases up to $\sim$1 K at lower current.

5. Conclusions and perspective

We have modeled with the M&M code a subset of the T_{cs} tests performed on conductor 1A of the CSMC in April–May 2000, for three different currents (30, 40, and 46 kA).

For the shots at 30 and 40 kA the last few thousand seconds of the evolution were considered, including the development of the voltage across the coil to the 0.5 mV threshold, which defines T_{cs}. For these cases the main emphasis was on the final temperature profiles along different conductors, for which boundary values proved to be in good agreement with experimental data.

For the shot at 46 kA the full evolution of the $\sim 10^4$ s transient from nominal initial conditions was followed, including the final transient of normal zone

[5] Although the manufacturer of the valve provided a characteristic with the ξ of the valve depending only on the valve lift [31], which was kept constant during this shot, we estimated the experimental data of mass flow rate through the valve as $2*(\text{MCI\_FCT\_01AO} + \text{MCI\_FCT\_02AO})$, and used the pressure drop between valve inlet (MCI_PT_01AO) and outlet of the inner module (CSV_PT_PC-CS1X), to obtain an effective characteristic, resulting in the time-dependent head loss factor shown in Fig. 12(g).

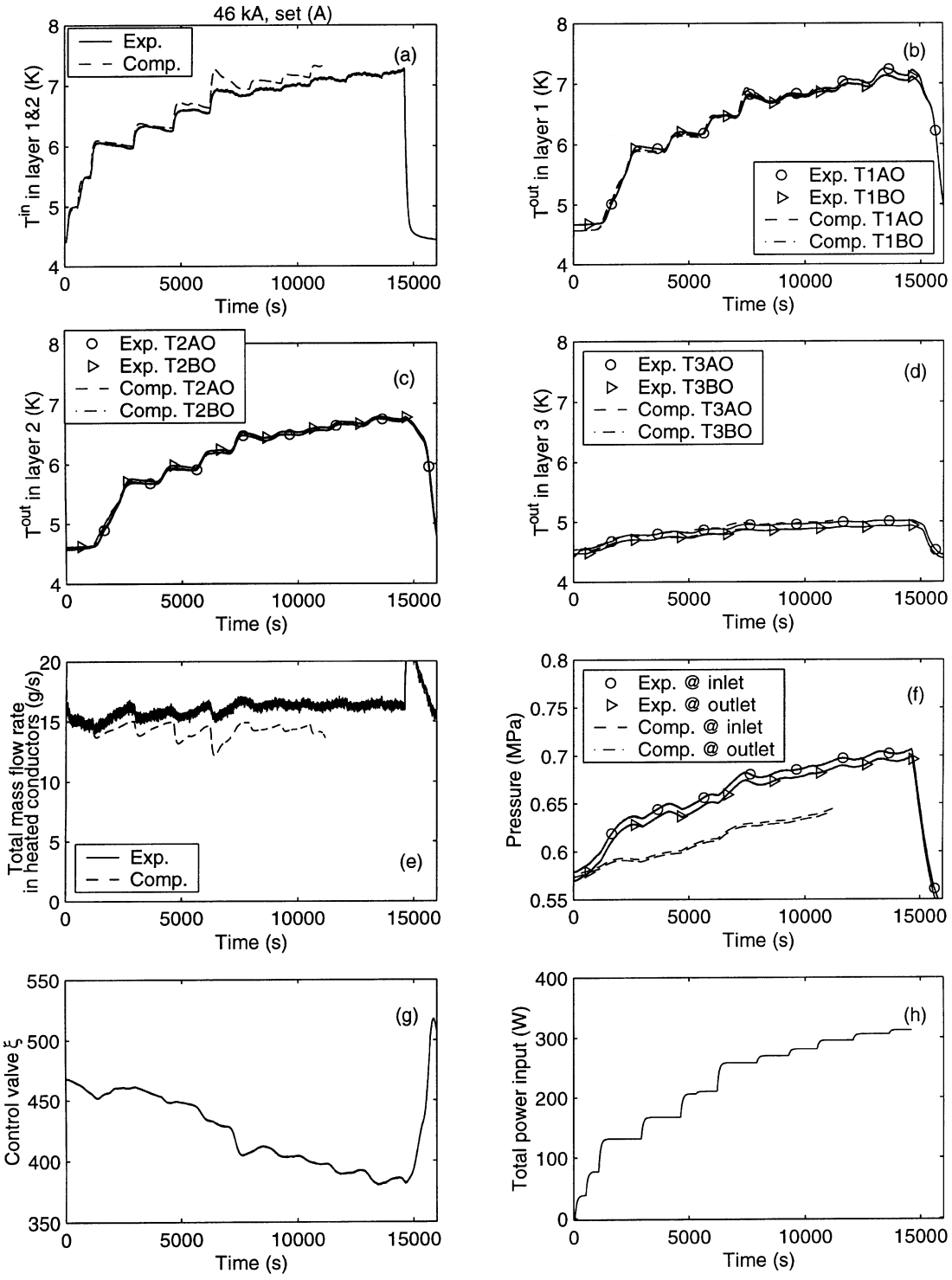

Fig. 12. T_{cs} measurement at $I = 46$ kA. Result of the simulation performed with the winding model in Fig. 3(c) and set (A). (a) Computed T_{in} (dashed), compared with the experimental signal from MCI_TS_01AI (solid). (b) Computed temperature at the outlet of 1A (dashed) and 1B (dash-dotted), compared to the experimental signal from MCI_TS_01AO (○) and MCI_TS_01BO (▷). (c) Computed temperature at the outlet of 2A (dashed) and 2B (dash-dotted), compared to the experimental signal from MCI_TS_02AO (○) and MCI_TS_02BO (▷). (d) Computed temperature at the outlet of 3A (dashed) and 3B (dash-dotted), compared to the experimental signal from MCI_TS_03AO (○) and MCI_TS_03BO (▷). (e) Evolution of the computed total mass flow rate in heated conductors (dashed), compared to the total measured mass flow rate (sum of the signals from MCI_FCT_01AI, MCI_FCT_01BI, and MCI_FCT_02A02BI (solid)). (f) Evolution of the computed pressure at the inlet (dashed) and outlet (dash-dotted) of the heated conductors, compared to the experimental signals from MCI_PT_01AI (○) and MCI_PT_01AO (▷). (g) Evolution of the head loss factor in the valve CV2 in Fig. 3(c) based on experimental data, used for the simulation. (h) Evolution of the total power input used in the simulation in the heaters common to layers 1–2.

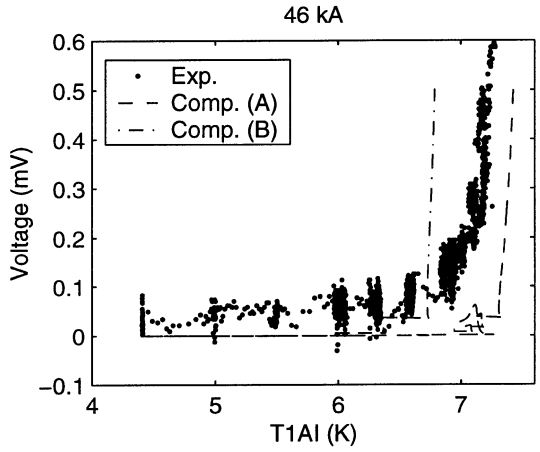

Fig. 13. T_{cs} measurement at $I = 46$ kA: computed voltage drop along conductor 1A, as a function of the temperature at conductor inlet, after the heaters. The results obtained using set (A) (dashed) and set (B) (dash-dotted) of critical current parameters (see text) are compared with experimental data obtained from voltage sensor MCI_VD_01A and temperature sensor MCI_TS_01AI (•).

Table 1
Summary of simulation results for different critical current parameter sets (A) or (B), see text, and for different transport current

	Current (kA)		
	30	40	46
Exp. T_{in} (K)	12.2	9.1	7.23
Exp. T_{out} (K)	10.1	8.4	7.21
Exp. $(T_{in} + T_{out})/2$ (K)[a]	11.1	8.7	7.2
(A)			
T_{cs} (K)[b]	11.9–12.4	–[c]	7.2–7.3
x (m)[d]	7–12	–[c]	39–51
(B)			
T_{cs} (K)[b]	11.5–12.1	8.3	6.5–6.7
x (m)[d]	7–12	33–48	32–45

[a] *Simplistic estimate* of T_{cs} obtained as average between the experimental T_{in} and T_{out}.
[b] Values of T_{cs} at the fronts of the normal zone when voltage = 0.5 mV, *computed with M&M.*
[c] Threshold of 0.5 mV not reached in the simulation.
[d] Location of the fronts of the normal zone, *computed with M&M.*

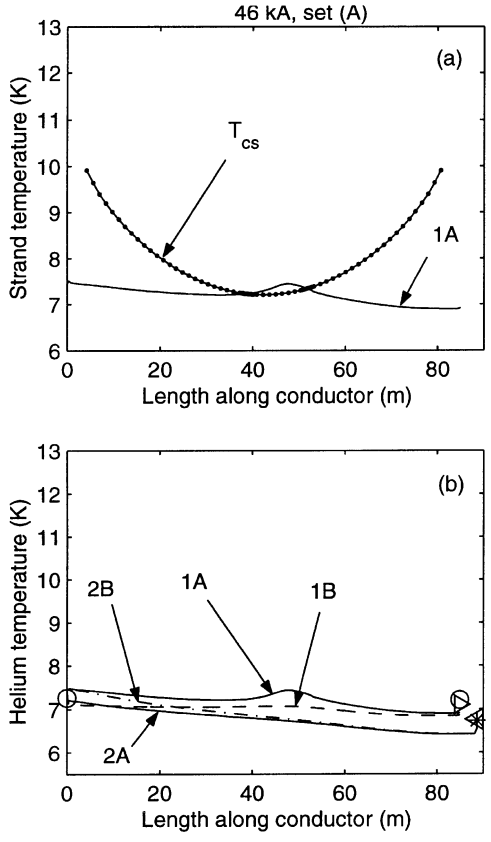

Fig. 14. T_{cs} measurement at $I = 46$ kA. Results computed using set (A). (a) Spatial profile of the strand temperature along conductor 1A (solid), at T_{cs} reached in the simulation. The profile of T_{cs} along the conductor is also reported (•). (b) Spatial profile of the average helium temperature along conductors 1A–2B at T_{cs} reached in the simulation, compared with temperatures measured at inlet, MCI_TS_01AI (○), and at outlet, MCI_TS_01AO (○), MCI_TS_01BO (▷), MCI_TS_02AO (∗) and MCI_TS_02BO (◁), in 1A, 1B, 2A, 2B, respectively, at T_{cs} reached in the experiment.

initiation, as a first example of multiple-time-scale analysis of thermal-hydraulics in superconducting coils. Good agreement was found over the whole transient in the evolution of inlet and outlet temperatures and flow rates in the first layers, provided a sufficiently accurate and indeed relatively sophisticated model is used for the cryogenic circuit and for the winding of the CSMC.

In all cases the agreement on the short-term voltage evolution, presently only qualitative, should be improved, which may require a more detailed model for the current distribution in the conductor cross-section.

In perspective we aim at analyzing quench propagation in the CSMC.

Acknowledgements

The European Fusion Development Agreement (EFDA) and the Italian Ministry for University and Scientific and Technological research (MURST) have partially financially supported this work. We wish to thank JAERI, Naka, Japan, and the Head of the Superconducting Magnet Laboratory, H. Tsuji, for giving us the opportunity to participate in the CSMC tests as members of the European Home Team, and for very kind hospitality. The availability and spirit of collaboration of many colleagues, in particular T. Kato, Y. Takahashi, Y. Nunoya, T. Ando, M. Takayasu, P. Michael, M. Ricci, and N. Mitchell, are also gratefully acknowledged. Finally, special thanks are due to N. Martovetsky who introduced us to the CSMC problems with first-hand, first-hour knowledge of them.

References

[1] Tsuji H, et al. ITER central solenoid model coil test program, 1998. Presented at the 17th IAEA Fusion Energy Conference.

[2] Mitchell N, et al. ITER CS model coil project. In: ICEC16 Proceedings, Elsevier, Amsterdam 1997. p. 763.

[3] Salpietro E. ITER toroidal field model coil (TFMC) design and construction. Fus Technol 1998;34:797.

[4] Komarek P, Salpietro E. The test facility for the ITER TF model coil. Fus Eng Des 1998;41:213.

[5] Takahashi Y, et al. Test results of ITER model coil – 13 T – 640 MJ Nb3Sn pulse coil. Jpn Cryogen Eng 2000;35:357 (in Japanese).

[6] Tsuji H, et al. Progress of the ITER central solenoid model coil program. Paper IAEA-CN-77/ITER/4 in: 18th IAEA Fusion Energy Conference, 2000 October 4–10; Sorrento, Italy.

[7] Zanino R, Marinucci C. Heat slug propagation in QUELL. Part I: experimental setup and 1-fluid GANDALF analysis. Cryogenics 1999;39:585.

[8] Zanino R, Marinucci C. Heat slug propagation in QUELL. Part II: 2-fluid MITHRANDIR analysis. Cryogenics 1999;39:595.

[9] Zanino R, Bottura L, Marinucci C. Computer simulation of quench propagation in QUELL. Adv Cryo Eng 1998l;43:181.

[10] Bottura L, Rosso C. Hydraulic network simulator model. Internal Cryosoft Note, CRYO/97/004, 1997.

[11] Marinucci C, Bottura L. The hydraulic solver Flower and its validation against the QUELL experiment in SULTAN. IEEE Trans Appl Supercond 1999;9:616.

[12] Savoldi L, Bottura L, Zanino R. Simulations of thermal-hydraulic transients in two-channel CICC with self-consistent boundary conditions. Adv Cryo Eng 2000;45:697.

[13] Zanino R, Santagati P, Savoldi L, Marinucci C. Joint + conductor thermal-hydraulic experiment and analysis on the full size joint sample using MITHRANDIR 2.1. IEEE Trans Appl Supercond 2000;10:1110.

[14] Zanino R, Savoldi L. Test and modeling of heat generation and heat exchange in the full size joint sample. In: Proceedings of the 18th International Cryogenic Engineering Conference (ICEC18), 2000 February 21–25; Narosa, New Delhi, 2000, p. 363.

[15] Savoldi L, Zanino R, Michael P. Tests and simulation of thermal-hydraulic transients in the US prototype joint sample, Int J Mod Phys B 2000 [to appear].

[16] Zanino R, Martovetsky N, Savoldi L. Pretest analysis of T_{cs} measurements in the central solenoid model coil. In: Proceedings of the 18th International Cryogenic Engineering Conference (ICEC18), 2000 February 21–25; Narosa, New Delhi, 2000, p. 195.

[17] Savoldi L, Zanino R. M&M: multi-conductor Mithrandir code for the simulation of thermal-hydraulic transients in superconducting magnets. Cryogenics 2000;40:179.

[18] Martovetsky N. Temperature profile in layer 1A during T_{cs} measurements. LLNL Memo, 2000 May 18 [unpublished].

[19] Kato T, et al. First test results for the ITER central solenoid model coil, 2000. In: 21st Symposium On Fusion Technology, 2000 September 10–15; Madrid, Spain. Submitted to Fus Eng Des.

[20] JAERI ITER Japanese Home Team. Procedure for CS model coil and CS insert testing (Revision 1). Report JASC-00-128, 21 February 2000 [unpublished].

[21] Martovetsky N. Distribution of magnetic field in CSMC and CS insert. LLNL Memo, 29 December 1999 [unpublished].

[22] JAERI ITER Japanese Home Team. Database of CSMC and CS insert. JAERI Memo 12-046, March 2000 [unpublished].

[23] Mitchell N. Minutes of the meeting on analysis work for CS model coil, 1 October 1998, Villigen, Switzerland [unpublished].

[24] Takigami H, Mitchell N, Okuno K, et al. Predicted thermohydraulic performance of the ITER central solenoid model coil conductors. IEEE Trans Appl Supercond 2000;10:1070.

[25] Savoldi L, Zanino R. Predictive study of current sharing temperature test in the Toroidal Field Model Coil using the M&M code. Cryogenics 2000;40:539–48.

[26] Nicollet S, Duchateau J-L, Fillunger H, et al. Dual channel cable in conduit thermohydraulics: influence of some design parameters. IEEE Trans Appl Supercond 2000;10:1102.

[27] Takahashi Y, Nunoya Y, Nishijima G, et al. Development of a 46-kA Nb_3Sn conductor joint for ITER model coils. Presented at the 16th International Conference on Magnet Technology, 1999 September 26–October 2; Tallahassee, FL, USA.

[28] Mitchell N. Steady state analysis of non-uniform current distributions in cable-in-conduit conductors and comparison with experimental data. Cryogenics 2000;40:99.

[29] Summers L, et al. A model for the prediction of Nb_3Sn critical current as a function of field, temperature, strain and radiation damage. IEEE Trans Magn 1991;27:2041.

[30] Mitchell N. Performance evaluations for the CSMC layer 1 with ramped temperature and constant conductor current, Release 2, 2000 June 5, and supplement, 2000 June 8 [unpublished].

[31] Kato T, Hamada K. Private communication; 2000.